2015 IEEE International Conference on Robotics and Automation (ICRA)
Washington State Convention Center
Seattle, Washington, May 26-30, 2015

Development and Experimental Validation of a Force Sensing Needle for Robotically Assisted Retinal Vein Cannulations

A. Gijbels, E.B. Vander Poorten, P. Stalmans, D. Reynaerts

***Abstract*— Retinal Vein Occlusion is a common retinal vascular disorder which can cause severe loss of vision. Retinal vein cannulation and subsequent injection of anti-coagulant in the affected vein is a promising treatment. Given the scale and the fragility of retinal veins on one side and the surgeons limited positioning precision and force perception on the other side, this procedure is considered too risky to perform manually at the moment. The paper tackles the limited force perception problem. The development of a novel force sensing cannulation needle based on Fiber Bragg Gratings is reported. The design, the calibration method and the experimental characterization of the produced force sensor are discussed. The functionality of the needle is validated by measuring puncture forces during cannulations in a custom-made retina model.**

I. Introduction

A. Retinal Vein Occlusion and retinal vein cannulation

Retinal surgery is considered as an extremely challenging type of surgery because of the scale and the fragility of the retinal anatomy. For some diseases, such as Retinal Vein Occlusion (RVO), the most promising procedure is even too difficult and risky to perform, forcing the surgeons to rely on less effective procedures. RVO is an eye condition which affects an estimated 16.4 million people worldwide [1]. It is the second most common retinal vascular disorder after diabetic retinal disease. The disease occurs when clots are formed in a retinal vein (Fig. 1). This causes the patient to slowly lose his/her sight. Today, there is no proven effective treatment clinically available for this disease [2]. A promising treatment is retinal vein cannulation (Fig. 1). During this procedure, the surgeon's objective is to inject an adequate dose of t-PA, a clot-dissolving agent, directly into the occluded retinal vein. A surgical microscope is placed above the patient's eye in order to have visual feedback on the surgical scene. Several research groups previously reported on successful cannulations in animal and human models [3], [4]. However, due to safety issues, the procedure is not performed clinically today. The needle must be inserted into a fragile vein with a diameter of only 400 µm or smaller [5] and kept there for several minutes before the fluid is fully injected. The limited positioning precision and force perception of the surgeon make it extremely difficult to correctly insert and keep the needle inside the vein without damaging it. Surgeons suffer from physiological tremor. Riviere et al. [6] reported on rms tremor amplitudes in the order of 180 µm. Gupta et al. [7] showed that 75 % of the interaction forces between the instrument and the retina are lower than 7.5 mN. The surgeon can only feel these forces in 19 % of the cases. This demonstrates that retinal surgeons mainly rely on visual feedback for these tasks.

Andy Gijbels, Emmanuel Benjamin Vander Poorten and Dominiek Reynaerts are with the Department of Mechanical Engineering, University of Leuven, 3001 Heverlee, Belgium

Peter Stalmans is with the Department of Ophthalmology, University of Leuven, 3000 Leuven, Belgium

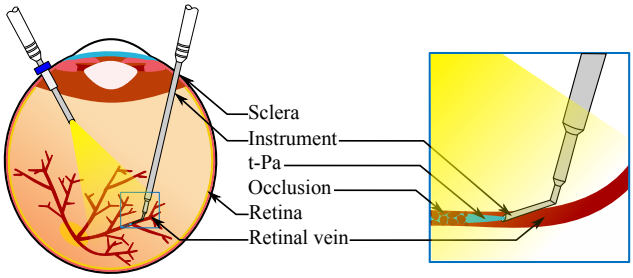

Fig. 1. Retinal Vein Cannulation: a hollow needle is inserted through the sclera and used to inject a clot-dissolving agent into an occluded vein which is causing RVO.

B. Robotic assistance for retinal surgery

A fair number of robotic systems for retinal surgery have been reported in literature [8]–[14]. The authors previously reported on the development of a robotic comanipulation system [15] and a telemanipulation system [16] for retinal surgery (Fig. 2). It was shown that independent of the system used it was feasible to significantly increase the positioning precision during a positioning task in an eye simulator [17]. This work reports on the development of a force sensing needle to provide robotic assistance during the actual puncture of the vein.

C. Force sensing instruments for retinal surgery

Ergeneman et al. [18] investigated forces during in vivo punctures of vessels in the CAM membrane of fertilized chicken eggs using a commercially available force sensor. This membrane was previously shown to be a good model for the human retina [19]. Force magnitudes ranging from 2 mN to 15 mN are reported for cannulations of targeted vessel diameters (100 µm-400 µm). A sudden drop in force level was found to mark the puncture event. Since the puncture forces are mostly below the perceptible level and also visual information is not conclusive, there is a high risk of a double puncture of the occluded vein. With a force sensing needle in place, the moment of first puncture could potentially be detected. Auditory and/or event-based force feedback [20] from the comanipulation or telemanipulation device could potentially be organised to assist the surgeon in preventing a double puncture. Despite the potential benefits, a force

978-1-4799-6923-4/15/$31.00 ©2015 IEEE

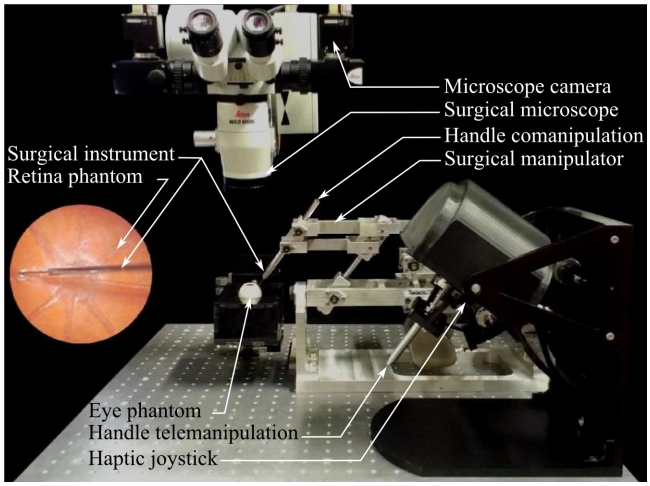

Fig. 2. The developed robotic comanipulation and telemanipulation system for retinal surgery [15]–[17].

sensitive cannulation needle was only successfully developed recently, mainly because of manufacturing problems. First, it is extremely difficult to produce a needle with a tip diameter small enough to cannulate the targeted veins. Second, the force sensor should be integrated into that portion of the needle which is inside the eye ball during the cannulation. This is because for a handle-mounted force sensor it would be practically impossible to distinguish the cannulation force at the tip of the needle from the contact force at the sclera. Latter force is typically an order of magnitude higher [21]. Iordachita et al. previously reported on the development of a force sensing pick instrument for retinal peeling, which is another challenging retinal procedure [22]. The group successfully integrated a sensor consisting of a flexure and four FBG optical fibers (Fiber Bragg Grating, i.e. optical strain gauges) inside the tip of the instrument. FBG optical fibers are thin (100 µm-200 µm diameter), extremely precise, stable, easy to sterilize and immune to electrical noise. As such they are ideal for the intended force sensing cannulation needle. The authors were the first to develop such a needle and previously reported briefly on its design [23]. Researchers from Johns Hopkins University recently reported on an alternative force sensing needle design, independently from the authors earlier work [24]. This work discusses the development of the instrument in more detail. Also, a more extensive validation of the instrument was conducted. Firstly, the design specifications and the design will be discussed. Secondly, an automated calibration procedure is developed and applied to the sensor. Thirdly, the sensor is fully characterized and shown to meet all design specifications. Lastly, puncture experiments are conducted on a custom-made polymer retina model. It is shown that the sensor is able to consistently detect puncture events in this model.

II. Development of a 2-DOF FBG Force Sensor

This section describes the development of a force sensing cannulation needle based on FBG force measurement. The main design specifications, the actual design and the detailed

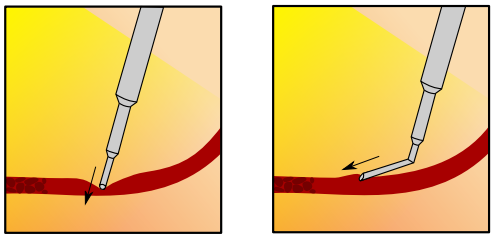

Fig. 3. (a) Using a straight needle can easily result in a double puncture since the vessel walls are pressed against each other. (b) Using a bended needle reduces the angle of attack and by such the risk of making a double puncture.

design of this novel instrument are consecutively being discussed.

A. Design specifications

Since the targeted vessels have a diameter ranging from 100 µm to 400 µm, a maximum allowable needle tip diameter of 80 µm is considered. For easy handling and good positioning precision the rest of the needle should be as rigid as possible and can have a larger diameter. The minimum diameter and length of the instrument shaft are therefore set to 0.5 mm and 30 mm respectively to conform to the state-of-the-art instruments for retinal surgery. Retinal surgeons suggested that cannulation would be simplified when the tip of the cannulation needle is bent under 45° with respect to the main axis of the tool shaft, compared to using straight needles. Figure 3 conceptually shows the effect of the tip angle (0° vs. 45°) on the cannulation. Indeed, when a straight needle is used, the vessel walls are pushed against each other when trying to access the lumen (Fig. 3(a)). A double puncture is in such case more likely to occur compared to the scenario where the vessel is approached under a certain angle (Fig. 3(b)). One can easily derive that in order to guarantee an intraocular force measurement during injections at all targeted locations on the human retina, the sensor should be integrated at a maximum distance of 18 mm from the tool tip. Clinicians further indicated that the predominant interest is to predict and detect the penetration event in a reliable and timely manner. While prediction capability is linked to sensor accuracy, detection relates to sensor resolution. Given reported minimal puncture forces of 2 mN an accuracy and precision of 0.2 mN are desirable. A maximum puncture force of 15 mN is assumed. The puncture event should be registered before the second puncture takes place. This mainly depends on the size of the targeted vessel and the relative speed of the needle, e.g. for a vein of 100 µm and a relative speed of 20 µm/s it still takes a couple of seconds to puncture the opposing vessel wall under some assumptions, including a 45° approach. However, a maximum registration period of 0.1 s is considered such that the delay goes unnoticed by the surgeon. Since injections can take up to 45 minutes [25], stability of the sensor must be guaranteed during this period. Finally, the hydraulic resistance of the needle should be minimal in order to minimize the injection

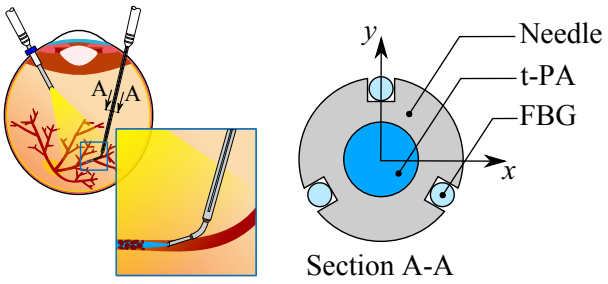

Fig. 4. The force sensing cannulation needle consists of an assembly of three tubes. Three FBG optical fibers are placed inside three grooves in the main shaft to provide a 2 DOF force measurement.

time. Table I summarizes the main design considerations.

TABLE I
MAIN DESIGN SPECIFICATIONS FOR A FORCE SENSITIVE CANNULATION NEEDLE.

Tip diameter	80 µm
Tip angle	45°
Shaft diameter	≥ 0.5 mm
Shaft length	≥ 30 mm
Force accuracy	0.2 mN
Force precision	0.2 mN
Force range	$\geq \pm 15$ mN
Registration time	≤ 0.1 s
Stability	≥ 45 min

B. Conceptual design

Figure 4 illustrates the concept of the envisioned force sensing cannulation needle. It is composed out of three stainless steel tubes which are inserted in one and another. The first tube is the tip which will be inserted into the vessel. The second tube acts as an interconnection between the tip and the shaft and is bended in order to create the desired angle of attack between the tip and the targeted vessel. The third tube is the main shaft. It consists of the FBG force sensor. Three FBG optical fibers are placed inside three parallel grooves that run down along the length of the main shaft. The shaft acts as the flexure of the force sensor. Lateral forces impose strains inside at least two of the fibers. The level of the strains is observed by the shift in wavelength of reflected light. Forces that are aligned with the main shaft's axis induce much smaller strains which are in fact found to be too small to detect. As described by Iordachita [22] for a retinal pick, an additional flexure could be foreseen to increase the axial force sensitivity. For a cannulation needle such flexure would bring additional difficulties in sealing the fluid channel, the axial force sensing is omitted. It is hypothesised here that the puncture force mainly acts along the axis of the tip. Under this assumption and for a bended tip such puncture force would cause a significant lateral force upon the main shaft. Knowing the geometric relation between cannulated vessel and cannulation needle one could in principle derive a relatively accurate estimate of the actual puncture force. Theoretically two FBGs are sufficient to measure the two components of the lateral force. However, as indicated in (1) aside from the strain ε, the FBG wavelength shift $\Delta\lambda$ is highly dependent on the temperature T. Typical values for sensitivities k_ε and k_T are 1.2 pm/µε and 12 pm/°C respectively. The third fiber is used to compensate for these temperature effects.

$$\Delta\lambda = k_\varepsilon \varepsilon + k_T \Delta T. \quad (1)$$

C. Detailed design

Figure 5(a) depicts a detail of the assembly of the tip tube and the bended tube, which will further be referred to as the needle insert. The needle tip has an outer and inner diameter of respectively 80 µm and 35 µm. Its length is only 5 mm in order to limit its hydraulic resistance. The tip has a bevel of 45° to facilitate the puncturing. The second tube is bended under a 45° angle. Both tubes are connected with glue. Figure 5(b) depicts the FBG force sensing needle. The inner

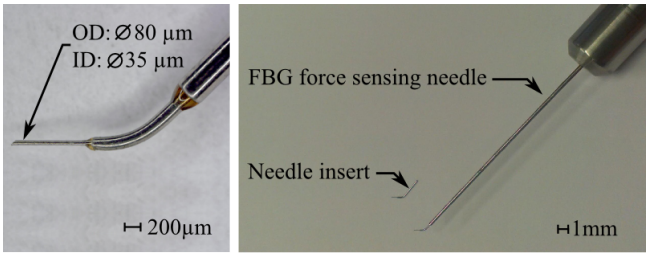

(a) (b)

Fig. 5. (a) A needle insert and the assembled force sensing needle. (b) A needle insert in detail.

and outer diameter of the shaft are dimensioned to obtain the specified force resolution and range. The relationship between the lateral forces F_x and F_y applied at the tip along the x- and y-axis (indicated on Fig. 4) and the induced strain ε_{ii} at the circumference of the tube is governed by

$$\varepsilon_{ii} = \frac{F_i d}{E I_{jj}} r, \quad \text{with} \quad i = x,y \quad \text{and} \quad j = y,x \quad (2)$$

where r is the radius of the tube, d is the distance between the tip and the location where the strain is measured, I_{jj} is the moment of inertia of the tube about the j-axis at this location and E is the Young's modulus of the material. The wavelength detection resolution and the scan frequency of the available interrogator (SM130-500 from Micron Optics) are respectively 2 pm and 500 Hz. The wavelength-to-strain sensitivity of commercially available FBG optical fibers is 1 pm/µε. Given these numbers and equation (2) it follows that a shaft with an outer and inner diameter of 0.55 mm and 0.25 mm respectively can be used to obtain a force resolution of 0.2 mN when a detection period of 0.1 s is expected. The tubes can easily withstand lateral forces of 20 mN without

plastic deformation. The grooves along the main shaft are dimensioned for 100 µm-diameter fibers. Figure 6 depicts the total instrument design. The tool handle is composed out of a top, central and bottom tube which are screwed in one and another. A 1 mm-diameter inner tube to supply the injection fluid runs through the handle to minimize the amount of dead volume and to leave space for the fibers to pass. While the bare fibers go through the bottom handle tube, the fibers leave the top handle with a protective polymer coating. At this side they are fixed with glue to release the fibers from any external tension put on the cabling.

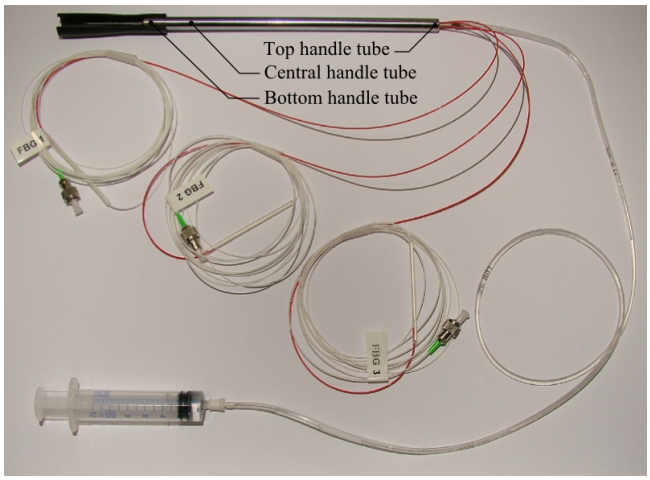

Fig. 6. The manufactured force sensing needle instrument

III. Calibration and Characterisation

This section describes the calibration of the sensor. Further, all design parameters related to the force measurement are analysed through experiments.

A. Calibration

The purpose of the calibration is to find a linearised relationship $\mathbf{C}$ between the lateral force components F_x and F_y and the reflected fiber wavelengths λ_1, λ_2 and λ_3:

$$\begin{bmatrix} F_x \\ F_y \end{bmatrix} = \mathbf{C} \begin{bmatrix} \lambda_1 \\ \lambda_2 \\ \lambda_3 \end{bmatrix}, \qquad \text{with} \qquad \mathbf{C} = \begin{bmatrix} C_{x1} & C_{x2} & C_{x3} \\ C_{y1} & C_{y2} & C_{y3} \end{bmatrix} \tag{3}$$

The components of the calibration matrix $\mathbf{C}$ can be determined by putting different weights on the needle tip when the instrument is held horizontally. From the registration of the wavelengths under n loads the coefficients of $\mathbf{C}$ can be solved from a set of n linear equations using a least squares fitting algorithm:

$$\begin{bmatrix} F_{i_1} \\ F_{i_2} \\ \vdots \\ F_{i_n} \end{bmatrix} = \begin{bmatrix} \lambda_{1_1} & \lambda_{2_1} & \lambda_{3_3} \\ \lambda_{1_2} & \lambda_{2_2} & \lambda_{3_3} \\ \vdots & \vdots & \vdots \\ \lambda_{1_n} & \lambda_{2_n} & \lambda_{3_n} \end{bmatrix} \begin{bmatrix} C_{i1} \\ C_{i2} \\ C_{i3} \end{bmatrix}, \qquad \text{with} \qquad i = x, y \tag{4}$$

To simplify the calibration process and to increase its precision, the procedure is automated. An actuated rotation module is developed to rotate the instrument about its longitudinal axis (Fig. 7). By such the x- and y-axis of the

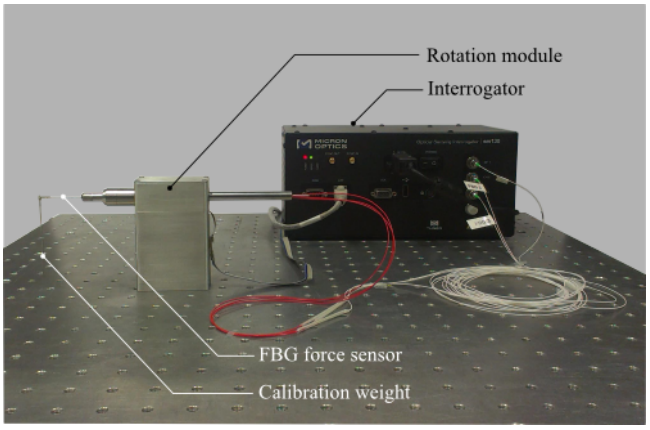

Fig. 7. An actuated rotation module is designed to automate the calibration procedure.

sensor are rotated and sinusoidically loaded when a constant weight is suspended at the tip of the instrument:

$$\begin{aligned} F_x &= +F_c \sin(\theta), \\ F_y &= -F_c \cos(\theta). \end{aligned} \tag{5}$$

where F_c is the applied load. A calibration weight of 2 g is used. The instrument is rotated in steps of 1°. When the calibration weight (pendulum-like behaviour) is stabilized after each step, 1000 wavelength samples are recorded and averaged for each fiber. The 360 resulting mean wavelengths for each fiber are used for the least squares fitting.

B. Characterisation

Figure 8(a) depicts the absolute value of the relative wavelengths as a function of the rotation angle. The relative wavelength Λ_i of fiber i is defined as:

$$\Lambda_i = \frac{\lambda_i - \widetilde{\lambda_i}}{\lambda_{i,max} - \widetilde{\lambda_i}} \tag{6}$$

where $\widetilde{\lambda_i}$ is the median of all measured wavelengths of fiber i. From this figure a larger noise level on FBG 1 can be observed compared to FBG 2 and FBG 3. This could be explained due to a certain anomaly during the assemby process. Figure 8(b) compares the modeled force from the calibration to the real force applied at the tip. It can be seen that the accuracy and precision of the model are slightly lower in the direction of FBG 1. Figure 9(a) and 9(b) quantify the accuracy and precision of the model. The precision can be improved by filtering the wavelengths with a moving average filter, with the consequence of a longer measurement period T_s. The graphs show that the specified force accuracy and precision can be met for a measurement period of 0.1 s when the needle insert is placed along the 30° direction. Figure 10(a) and 10(b) show the relationship between the applied and calculated force when a cyclic load as described above is applied along the x- and y-axis respectively. These graphs show that the sensor has a

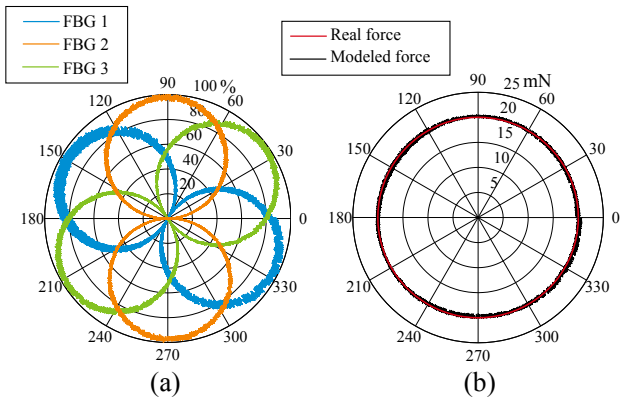

Fig. 8. (a) Absolute relative wavelengths measured during sensor calibration as a funtion of rotation angle. (b) Comparison between the modeled force and the real applied force at the tip of the needle. The precision is a function of the registration period T_s.

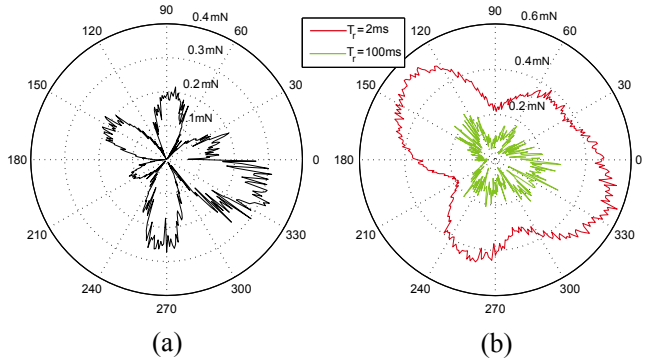

Fig. 9. (a) Accuracy and (b) precision of the measured force for a suspended weight of 2 g. By lengthening the measurement window from 2 ms to 100 ms the obtained precision improves to approximately 0.2 mN. Accuracy is not affected by a longer measurement window.

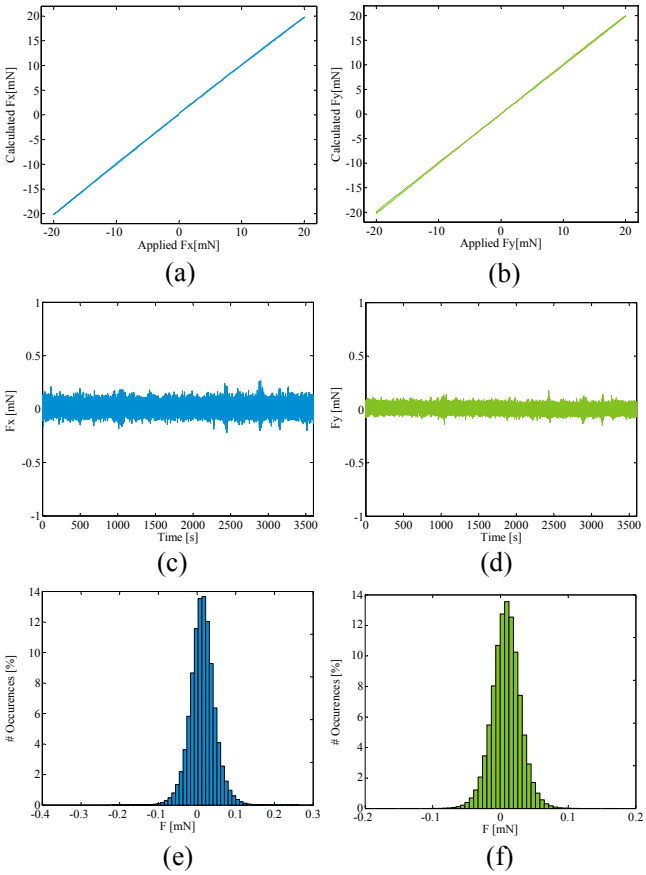

Fig. 10. (a)+(b) Relationship between the applied and modeled forces F_x and F_y under cyclic loading. (c)+(d) Measured F_x and F_y force for a one hour registration period. (e)+(f) Histograms of the F_x and F_y residual errors for a one hour measurement cycle.

high repeatibility and minimal non-linearities and hystersis. This validates the use of a linear model. Next, the stability of the sensor was tested by measuring the wavelengths for an hour while the force sensor remained unloaded. Figure 10(c) and 10(d) depict the calculated forces F_x and F_y. From these graphs it can be seen that the sensor drift is negligible. The histograms of figure 10(e) and 10(f) show that residual errors are in general smaller than 0.1 mN during 60 minutes. Lastly, the effect of the change in temperature that can be expected when entering the eye with the needle is simulated. For this purpose the force sensor, at room temperature, is immersed perpendicularly into water with a temperature of 37 °C. The instrument is gently moved at a constant speed of 10 mm/s into the water by a linear drive mechanism (Fig. 11). In this way disturbance forces when entering the water are minimised so that it becomes possible to focus on the temperature effect. Figure 12(a) shows the relative wavelength shift of the fibers. Because the fibers heat up at different rates and there is a slight difference in location of the gratings an apparent lateral force is registered (Fig. 12(b)). The time constant for stabilization of the sensor readout is 3 s. This is acceptable since it takes more than 3 s

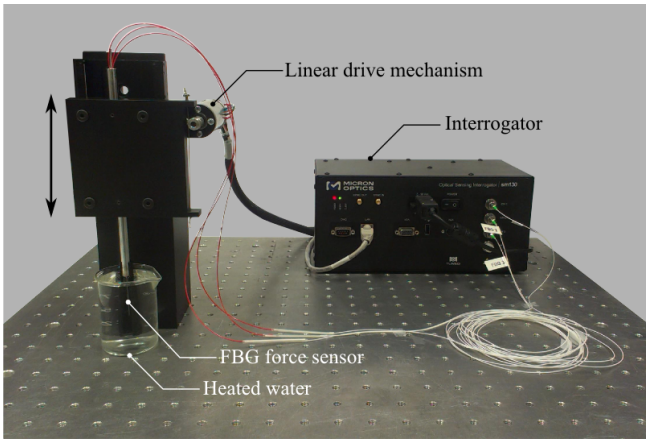

Fig. 11. The force sensing needle is immersed into water at 37° temperature by a linear drive mechanism to simulate the effect of a temperature shock when entering the patient's eye.

to carefully approach the retina once inside the eye. Thus, at the moment of puncture the effect of the temperature shock on the force readings can be ignored.

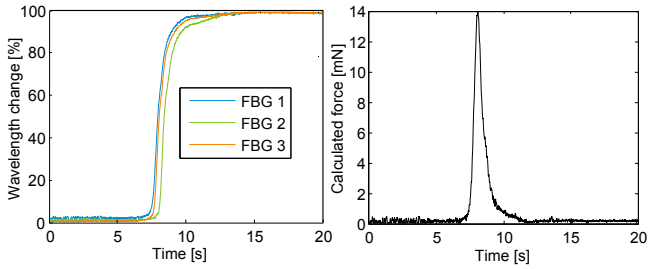

Fig. 12. (a) Normalized wavelength shift of the fibers for a 15 °C temperature shock. (b) The apparent lateral force observed from this temperature shock.

IV. Experiments

This section aims at verifying that the developed force sensing cannulation needle allows puncturing and successful detection of the puncturing process. For this purpose a retina model is used which was previously developed by the authors (Fig. 13(a)) [15]. The model consists of radial beam-shaped channels with a width ranging from 120 µm to 500 µm. When fluid is succesfully injected into a channel of the retina model, it flows towards the center of the retina where it can exit the sample through a central tube. The retina samples are made out of PDMS, a heat-curable flexible polymer, using a mold (Fig. 13(b)) and a spincoating process to seal the top part. The PDMS is prepared by mixing Sylgard 184 elastomer and a curing agent. From multiple trials it was shown that a weight ratio of 10/1 results in puncture forces that are comparable to those of alternative biological models that are typically used.

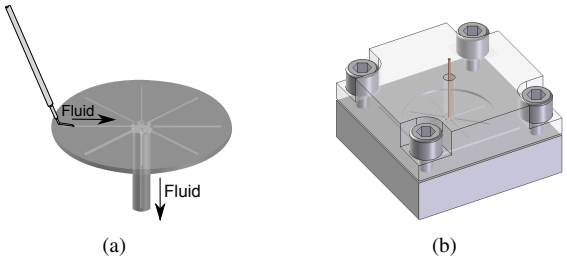

Fig. 13. A PDMS retina mock-up (a) was made by pouring a mixture of PDMS elastomer and a curring agent into a hot mold (b). The top of the retina is closed by a spin coating procedure. The retina consists of 80 µm-500 µm beam-shaped channels which simulate retinal veins.

As a preliminary test, one user punctured five channels of a PDMS retina. For this purpose a test setup was developed to move the force sensing needle relative to the channels (Fig. 14). First, a passive linear and rotation stage are used to set respectively the height and the angle of attack of the needle tip with respect to the targeted channel (Fig. 15). Next, the tip is moved in a steady manner along its axis by means of an actuated linear stage. The actuation speed is set to 0.4 mm/s. The user controls the motion direction with two foot pedals. Figure 16 depicts the measured forces during

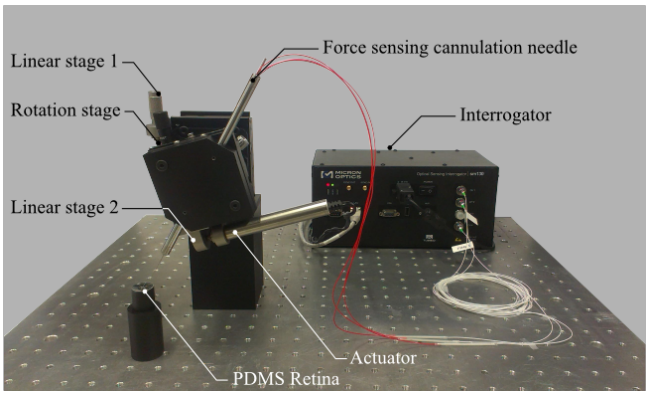

Fig. 14. Setup to position the tip of the needle with respect to a channel of a PDMS retina. The upward and downward movement of the tip are controlled with passive linear stage 1. The angle of attack is set by means of a rotation stage. The movement along the main axis of the tip is regulated with actuated linear stage 2.

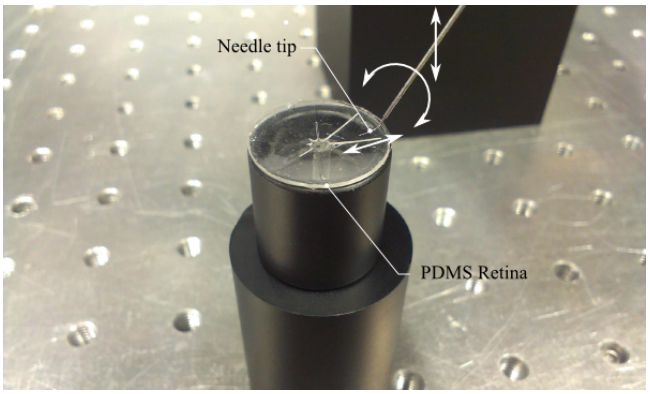

Fig. 15. Degrees of freedom of the tip of the needle with respect to the PDMS retina.

the experiment and the type of motion being applied. The sudden drop in force level when a force of 6 mN is reached, indicates the puncture. Note that the force doesn't drop to zero until the tip is retracted. Further, it is hypothesised that a pulling force is needed to break away from the vessel wall. The repeatability of the process suggests that it would be feasible to derive detection algorithms to automatically detect the different phases of the cannulation process.

V. Conclusion and Future Work

This work reported on the development of a novel FBG force sensing needle instrument to assist surgeons during a retinal vein cannulation. The needle is foreseen of three FBG optical fibers which are integrated into an assembly of three stainless steel tubes. An automated calibration method was presented and through experiments it was shown that all design parameters are met. The accuracy and precision of the force sensor are 0.2 mN for a measurement window of 100 ms and the sensor stabilizes after 3 s when exposed to a 15 °C temperature rise. A PDMS retina model was

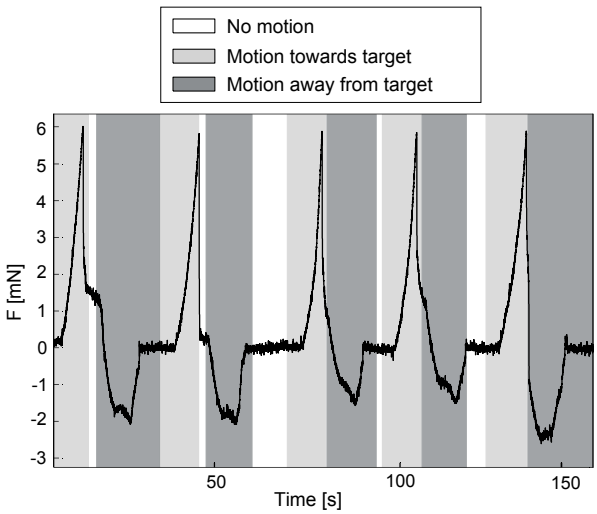

Fig. 16. Measured force levels during five consecutive punctures in a PDMS retina.

selected to simulate the punctures. Using these models, it was shown that with the instrument it is possible to reliably detect puncture events. In the future, the sensor will be used to investigate event-based force feedback to maximise the success ratio for retinal vein cannulations, using the developed robotic platforms for retinal surgery.

VI. Acknowledgments

This research is funded by the EU-funded project EurEyeCase in the framework of the H2020 funding scheme, an industrial research fund from the University of Leuven and a PhD grant from the Institute for the Promotion of Innovation through Science and Technology in Flanders (I.W.T.-Vlaanderen), 101445.

References

[1] S. Rogers, "The prevalence of retinal vein occlusion: Pooled data from population studies from the united states, europe, asia, and australia," *Ophthalmology*, vol. 117, pp. 313– 319, 2010.

[2] B. Nilufer and B. Cosar, "Surgical treatment of central retinal vein occlusion," *Acta Ophthalmologica*, vol. 86, pp. 245–252, 2008.

[3] J. Weiss and L. Bynoe, "Injection of tissue plasminogen activator into a branch retinal vein in eyes with central retinal vein occlusion," *Ophthalmology*, vol. 108-12, pp. 2249–2257, 2001.

[4] L. A. Bynoe, R. K. Hutchins, H. S. Lazarus, and M. A. Friedberg, "Retinal endovascular surgery for central retinal vein occlusion: Initial experience of four surgeons," *Retina*, vol. 25, pp. 625–32, 2005.

[5] F. Skovborg, V. Nielsen, E. Lauritzen, and O. Hartkopp, "Diameters of the retinal vessels in diabetic and normal subjects," *Diabetes*, vol. 18(5), pp. 292–298, 1969.

[6] C. N. Riviere and P. S. Jensen, "A study of instrument motion in retinal microsurgery," *Proc. of the 22nd Annual EMBS Int. Conf.*, 2000.

[7] P. Gupta, P. Jensen, and E. Juan, "Surgical forces and tactile perception during retinal microsurgery," *Proc. of the Second Int. Conf. on Medical Image Computing and Computer Assisted Intervention (MICCAI)*, pp. 1218–1225, 1999.

[8] S. Yang, R. A. MacLachlan, and C. N. Riviere, "Design and analysis of 6 dof handheld micromanipulator," *Proc. IEEE Int. Conf. on Robotics and Automation (ICRA).*, pp. 1946 – 1951, 2012.

[9] A. Uneri, M. Balicki, J. Handa, P. Gehlbach, R. Taylor, and I. Iordachita, "New steady-hand eye robot with microforce sensing for vitreoretinal surgery research," *Int. Conf. on Biomedical Robotics and Biomechatronics*, pp. 814–819, 2010.

[10] W. Wei, R. Goldman, N. Simaan, H. Fine, and S. Chang, "Design and theoretical evaluation of micro-surgical manipulators for orbital manipulation and intraocular dexterity," *ICRA*, pp. 3389–3395, 2007.

[11] S. Charles, H. Das, T. Ohm, C. Boswell, G. Rodriguez, R. Steele, and D. Istrate, "Dexterity-enhanced telerobotic microsurgery," *Proc. of the IEEE Int. Conf on Advanced Robotics*, pp. 5–10, 1997.

[12] A. Guerrouad and P. Vidal, "Smos: Stereotaxical microtelemanipulator for ocular surgery.," *Medicine and Biology Society*, pp. 879–880, 1989.

[13] H. Meenink, R. Hendrix, P. Rosielle, M. Steinbuch, and M. de Smet, "A master-slave robot for vitreo-retinal eye surgery," *Proc. of the 10th Int. Conf. of European Society for Precision Engineering and Nanotechnology*, 2010.

[14] M. Nasseri, M. Eder, S. Nair, E. Dean, M. Maier, D. Zapp, C. Lohmann, and A. Knoll, "The introduction of a new robot for assistance in ophthalmic surgery," *35th Annual Int. Conf. of the IEEE Engineering in Medicine and Biology Soc. (EMBC'13)*, 2013.

[15] A. Gijbels, N. Wouters, P. Stalmans, H. Van Brussel, D. Reynaerts, and E.B. Vander Poorten, "Design and realisation of a novel robotic manipulator for retinal surgery," *Proc. IEEE Int. Conf. on Intelligent Robots and Systems*, 2013.

[16] A. Gijbels., E.B. Vander Poorten, P. Stalmans, H. Van Brussel, and D. Reynaerts, "Design of a teleoperated robotic system for retinal surgery," *Proc. IEEE Int. Conf. on Robotics and Automation*, 2014.

[17] A. Gijbels, E.B. Vander Poorten, B. Gorissen, A. Devreker, P. Stalmans, and D. Reynaerts, "Experimental validation of a robotic comanipulation and telemanipulation system for retinal surgery," *Proc. IEEE RAS & EMBS Int. Conf. on Biomedical Robotics and Biomechatronics*, 2014.

[18] O. Ergeneman, J. Pokk, V. Pocepcova, H. Hall, J. Abott, and B.J. Nelson, "Characterization of puncture forces for retinal vein cannulation, journal of medical devices," *Journal of Medical Devices*, vol. 5, pp. 1–6, 2011.

[19] T. Leng, J. Miller, K. Bilbao, D. Palanker, P. Huie, and M. Blumenkranz, "The chick chorioallantoic membrane as a model tissue for surgical retinal research and simulation," *Retina*, vol. 24(3), p. 427434, 2004.

[20] K. Kuchenbecker, J. Fiene, and G. Niemeyer, "Event-based haptics and acceleration matching: portraying and assessing the realism of contact," in *Eurohaptics Conference, 2005 and Symposium on Haptic Interfaces for Virtual Environment and Teleoperator Systems, 2005. World Haptics 2005. First Joint*, pp. 381–387, March 2005.

[21] A. S. Jagtap and C. N. Riviere, "Applied force during vitreoretinal microsurgery with handheld instruments," *Proc. IEEE Eng. Med. Biol. Soc.*, vol. 4, pp. 2271–2773, 2004.

[22] X. He, J. Handa, P. Gehlbach, R. Taylor, and I. Iordachita, "A submillimetric 3-dof force sensing instrument with integrated fiber bragg grating for tetinal microsurgery," *IEEE Transactions on Biomedical Engineering*, vol. 61, pp. 522–534, 2014.

[23] A. Gijbels, S. Colson, D. Reynaerts, and E.B. Vander Poorten, "Design and manufacturing of a 2-dof force sensing needle for retinal surgery," *4th Joint Workshop on Computer/Robot Assisted Surgery*, 2014.

[24] B. Gonenc, P. Gehlbach, J. Handa, R.H. Taylor, and I. Iordachita, "Force-sensing microneedle for assisted retinal vein cannulation," *IEEE Sensors*, 2014.

[25] M. Tameesh, "Retinal vein cannulation with prolonged infusion of tissue plasminogen activator (t-pa) for the treatment of experimental retinal vein occlusion in dogs," *American Journal of Ophthalmology*, vol. 138(5), pp. 829–839, 2004.